Temperature Dependence of $(SCN)_2^{\bullet-}$ in Water at 25−400 °C: Absorption Spectrum, Equilibrium Constant, and Decay

Guozhong Wu, Yosuke Katsumura,* Yusa Muroya, Mingzhang Lin, and Tomomi Morioka

Nuclear Engineering Research Laboratory, School of Engineering, The University of Tokyo, Shirakata Shirane 2-22, Tokai-mura, Naka-gun, Ibaraki 319-1188, Japan

Received: January 4, 2001; In Final Form: January 15, 2001

The temperature dependence of the absorption spectrum of the formation and decay of $(SCN)_2^{\bullet-}$, a well-characterized dimer anion, was investigated at temperatures from 25 to 400 °C. The absorption peak was found to shift to longer wavelength with temperature (red shift), from 470 nm at 25 °C to 510 nm at 400 °C. The equilibrium constants K_1 and K_2 for the reactions $SCNOH^{\bullet-} \rightleftarrows SCN^{\bullet} + OH^-$ and $SCN^{\bullet} + SCN^- \rightleftarrows (SCN)_2^{\bullet-}$, respectively, were found to decrease with temperature. Due to the considerable decrease of K_2 with temperature, a rise in temperature shifts the reaction in favor of $SCN^{\bullet}$, so the observed yield of $(SCN)_2^{\bullet-}$ at high temperatures is strongly dependent on the SCN^- concentration. As the $SCN^{\bullet}$ concentration could be as high as or even higher than the $(SCN)_2^{\bullet-}$ concentration at high temperatures, a pseudo-first-order decay of $SCN^{\bullet}$ has to be taken into consideration to account for the overall decay of $(SCN)_2^{\bullet-}$. Using the kinetic parameters obtained in this work and available in the literature, the decay profiles of $(SCN)_2^{\bullet-}$ can be well reproduced for any temperature and KSCN concentration considered. A combination of the simulation and the experimental results reveals a decrease of ϵ_{max} of $(SCN)_2^{\bullet-}$ with temperature; the degree is ∼30% for a rise from 25 to 400 °C.

Introduction

The study of solute−solute and solute−solvent interactions in sub- and supercritical water is important for the application of supercritical water as a medium for chemical processing such as waste oxidation and hydrolysis as well as for the understanding of temperature effects on radical reactions in the field of water chemistry. Chemistry and kinetics of reactions in supercritical water may change considerably with even a small variation in temperature or pressure because water properties, for example, H-bonding and dielectric constant, are very sensitive to such variations. Spectroscopic methods are widely used to investigate the change of water properties and its subsequent effect on solvation processes of solutes. UV−vis spectroscopy,[1,2] Raman spectroscopy,[3] NMR,[4] and X-ray absorption fine structure[5] have been applied by many researchers in the study of supercritical water. Time-resolved spectroscopy is a more powerful technique because it enables one to follow rapid formation or decay processes of transient species on the time scale of nanoseconds to milliseconds, providing more detailed insights into chemical reactions. 2-Naphthol was used[6] as one probe molecule for the study of solute−solvent interactions. For this purpose its excited-state deprotonation in supercritical water is followed with time-resolved fluorescence spectroscopy. More recently, flash laser photolysis[7] and pulse radiolysis[8−11] techniques have been applied to the study of radical reactions in supercritical water. Hydrated electrons (e_{aq}^-) and $OH^{\bullet}$ generated from water radiolysis are active with many substances and secondary radicals are easily formed, so it is possible to study the solvent effect on radical reactions in detail as long as the newly formed radicals have optical absorption, which is strong enough for detection.

In our previous work[10] the temperature dependence of e_{aq}^- was studied over a wide temperature range. It was revealed that the absorption peak of e_{aq}^- shifted substantially to longer wavelength with temperature, and the spectrum was much broadened in supercritical water. Being the opposite of e_{aq}^-, the $OH^{\bullet}$ radical is a strong oxidizing species, and its direct observation is not convenient because its absorption band is in the ultraviolet region and the absorption coefficient is small (540 M^{-1} cm^{-1} at 188 nm[12]) at room temperature. The role of $OH^{\bullet}$ is important in water radiolysis, and it raises a corrosion problem in nuclear reactors. The $OH^{\bullet}$ can be converted to another type of oxidizing radical that is convenient for optical determination via the reaction with some inorganic ions, for instance, SCN^- and CO_3^{2-}. The oxidation of SCN^- by $OH^{\bullet}$ forms a dimer anion, $(SCN)_2^{\bullet-}$. At room temperature, this radical has a strong and broad absorption band centered at 472 nm and its lifetime is long. Because the absorbance of $(SCN)_2^{\bullet-}$ can be conveniently and accurately determined, N_2O-saturated 0.01 M KSCN aqueous solution is usually used as a standard reference in pulse radiolysis. Because the $(SCN)_2^{\bullet-}$ is an active species, rate constants for its reactions with many substances have been reported. Unlike the e_{aq}^-, the behavior of which at elevated temperatures has been extensively studied, there was only one paper by Elliot and Sopchyshyn[13] on the decay of $(SCN)_2^{\bullet-}$ over the temperature range of 15−90 °C. They found that the rate of decay was a function of temperature and SCN^- concentration and that the absorption coefficient of $(SCN)_2^{\bullet-}$ was independent of temperature over the temperature range of interest.

In this work, the behavior of $(SCN)_2^{\bullet-}$ was investigated over the temperature range of 25−400 °C covering the supercritical conditions. Temperature effects on the spectra, equilibrium

* Address correspondence to this author at the Nuclear Engineering Research Laboratory, School of Engineering, The University of Tokyo, Hongo 7-3-1, Bunkyo-ku, Tokyo 113, Japan (fax/telephone +81-3-5841-8624; e-mail katsu@q.t.u-tokyo.ac.jp).

10.1021/jp0100506 CCC: $20.00
Published on Web 04/26/2001

constants K_1 and K_2, and decay rates of $(SCN)_2^{\bullet-}$ were examined. The SCN^- concentration dependence of $(SCN)_2^{\bullet-}$ was observed to be more substantial at higher temperatures. The decay profiles of $(SCN)_2^{\bullet-}$ were reproduced well for any conditions using the known and some assumed kinetic parameters. A pseudo-first-order decay of the $SCN^{\bullet}$ radical is considered and included in the reaction scheme; its role is important at high temperatures or even at room temperature with very low SCN^- concentration. This work may also give a clue to the understanding of behavior of other dimer anions such as $Cl_2^{\bullet-}$, $Br_2^{\bullet-}$, and $I_2^{\bullet-}$ in high-temperature and supercritical water.

Experimental Section

KSCN and other chemicals were of reagent grade and used as supplied. Distilled water further filtered from a Millipore system was used for preparation of aqueous solutions. All of the KSCN solutions (1×10^{-4}−0.2 m) were at natural pH except that in some cases 0.01 m NaOH was added for the study of pH dependence. The KSCN solution was deaerated by bubbling N_2O so that the e_{aq}^- was rapidly converted to $OH^{\bullet}$. The solution was loaded to the irradiation cell by an HPLC pump with a flow rate of 3−4 mL/min, corresponding to a residence time of 6−8 s in the cell.

Details of the apparatus for pulse radiolysis were described elsewhere.[10] The high-temperature cell made of Hasteloy C273 can withstand temperatures up to 500 °C and pressures up to 500 atm, well beyond the critical point of water. The pulsed electron beam has an energy of 35 MeV, and its width was 50 ns. A pulsed xenon lamp was used in the optical detection system to generate light with strong intensity, and the optical length was 1.5 cm. The analyzing light exiting from the cell was focused and passed through a monochromator and then detected by a photodiode. The time-dependent signal was recorded with a digital oscilloscope. The dose per pulse at room temperature ranged from 25 to 50 Gy, determined using N_2O-saturated 0.01 M KSCN solution and a $G\epsilon\{(SCN)_2^{\bullet-}\}$ of 5.2×10^{-2} m^2/J at 472 nm.[14] Absorbed energy was corrected for density variation of water with temperature and pressure. The water density was taken from the equation of Hill.[15] The pressure−volume−temperature relationship of the KSCN solutions was assumed to be the same as that of pure water, and some consequent errors were allowed. The molal concentration (moles per kilogram) was used in the discussion of temperature effects, but in other cases the molar concentration (moles per liter) was used for convenience.

Results and Discussion

Temperature Dependence of Absorption Spectra. Figure 1 shows time profiles of $(SCN)_2^{\bullet-}$ observed at 480 nm for 0.01 m KSCN solution under various conditions. Absorption of $(SCN)_2^{\bullet-}$ was clearly observed up to the supercritical conditions, for example, 400 °C and 350 atm. The decay of $(SCN)_2^{\bullet-}$ is slow at room temperature and significantly enhanced by increasing the temperature. The lifetime in supercritical water is shorter by 2 orders of magnitude than in room temperature water. Also indicated is a decrease of the initial absorbance of $(SCN)_2^{\bullet-}$ with temperature due to the decrease of water density and changes of some relevant parameters concerned with $(SCN)_2^{\bullet-}$ formation, as will be discussed later in the text.

Figure 2 shows the temperature dependence of the absorption spectrum taken at the end of the pulse. As can be seen, the absorption peak shifts gradually to longer wavelength with temperature. The peak shifts from 470 nm at 25 °C (200 atm) to 510 nm at 400 °C (350 atm), corresponding to an energy

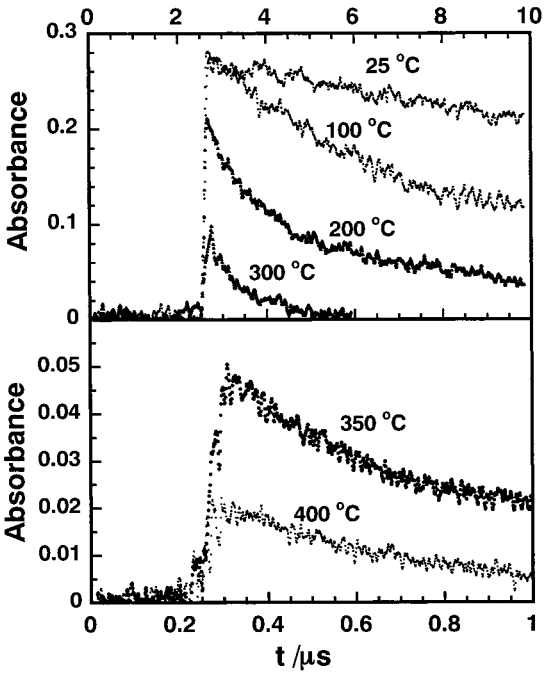

Figure 1. Temporal profiles of $(SCN)_2^{\bullet-}$ in 0.01 m KSCN solution, N_2O-saturated, dose = 35 Gy $pulse^{-1}$. Conditions: 25−200 °C, 200 atm; 300 °C, 250 atm; 350 °C, 300 atm; 400 °C, 350 atm.

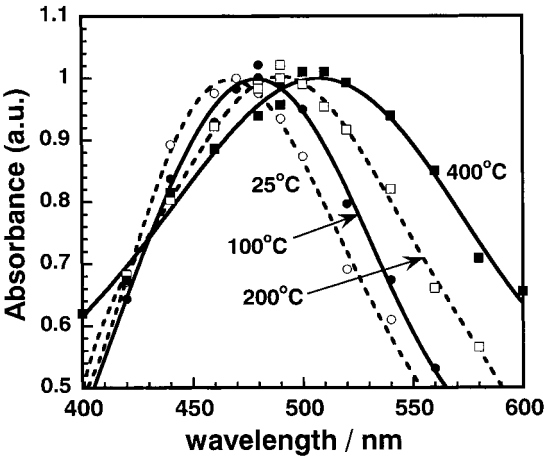

Figure 2. Normalized absorption spectra of $(SCN)_2^{\bullet-}$ at different temperatures. Conditions: [KSCN] = 0.01 m; 25−200 °C, 200 atm; 400 °C, 350 atm.

difference of 0.196 eV. The peak shift was ascertained by a number of repeated experiments. It is also noted that the absorption band of $(SCN)_2^{\bullet-}$ broadens with increasing temperature. The spectral change with temperature for $(SCN)_2^{\bullet-}$ is very similar to that for e_{aq}^-, although the change for e_{aq}^- is more remarkable.[10,16−18] The red shift of $(SCN)_2^{\bullet-}$ and e_{aq}^- with temperature is likely to be related to the decrease of polarity, H-bonding, and dielectric constant of water at high temperatures.

Temperature Dependence of $G\epsilon_{max}$ for 0.01 m KSCN Solution. Because the temperature dependence of the G value and ϵ_{max} has not been separately established, the product $G\epsilon_{max}$ was used to evaluate the radiation effect at high temperatures by taking a 0.01 m KSCN solution as an example. As shown in Figure 3, the $G\epsilon_{max}$ of $(SCN)_2^{\bullet-}$ increases with temperature up to 140 °C and then decreases continuously as the temperature is further increased. The value of $G\epsilon_{max}$ in supercritical water (400 °C, 350 atm) is less than one-fifth of that in room temperature water. The $G\epsilon_{max}$ in alkaline solution was also determined for comparison. With the addition of 0.01 m NaOH,

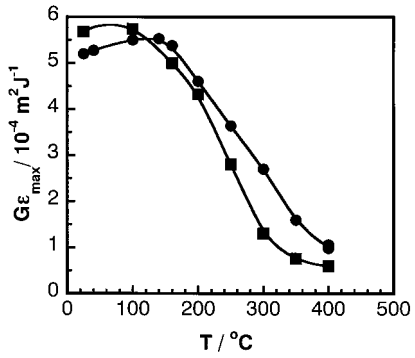

Figure 3. Plots of $G\epsilon_{max}$ as a function of temperature for $(SCN)_2^{\bullet-}$ in N_2O-saturated (●) 0.01 m KSCN and (■) 0.01 m KSCN plus 0.01 m NaOH solutions.

the $G\epsilon_{max}$ at room temperature is increased by ~10% due to the conversion of H atom to e_{aq}^- via the reaction $OH^- + H \rightarrow H_2O + e_{aq}^-$ and the subsequent conversion of e_{aq}^- to $OH^\bullet$ through the reaction with N_2O. The result is consistent with $G(OH^\bullet) = 0.63$[19] (N_2O saturation) and $G(H) = 0.06$ μmol/J in water. The $G\epsilon_{max}$ in alkaline solution is nearly constant up to 100 °C and then decreases with temperature. At temperatures >120 °C, the $G\epsilon_{max}$ in 0.01 m KSCN plus 0.01 m NaOH solution is always smaller than that in 0.01 m KSCN solution under otherwise identical conditions. Additionally, the decay of $(SCN)_2^{\bullet-}$ appears to be faster in the alkaline solution over the temperature range studied. However, no obvious spectral difference between the two systems was found.

KSCN Concentration Dependence of $(SCN)_2^{\bullet-}$ and Temperature Dependence of K_2. At room temperature, the $(SCN)_2^{\bullet-}$ yield was found[20,21] to increase with SCN^- concentration in the pulse radiolysis experiments due to the higher OH scavenging capacity of concentrated SCN^- solutions. However, this concentration dependence is not significant. It was shown[20] that the $(SCN)_2^{\bullet-}$ yield at 1.0×10^{-4} M SCN^- is nearly half of that at 0.01 M SCN^-, and the yield levels off at concentrations of 0.01−1.0 M. As already noted in Figure 3, the $G\epsilon_{max}$ for 0.01 m KSCN solution decreases considerably with temperature, indicating lower $(SCN)_2^{\bullet-}$ yield at high temperatures. However, the use of high SCN^- may result in a higher observable $(SCN)_2^{\bullet-}$ yield because the concentration dependence is probably more substantial in the high-temperature region. To confirm this speculation, the concentration dependence of $(SCN)_2^{\bullet-}$ was investigated in detail by varying the KSCN concentration.

Figure 4 shows the absorbance maximum of $(SCN)_2^{\bullet-}$ at 25−400 °C with KSCN concentrations ranging from 1×10^{-4} to 0.2 m. As is seen, the concentration dependence is actually more substantial at high temperatures than at room temperature. Leveling off of the $(SCN)_2^{\bullet-}$ yield at high concentrations is observed at 25 and 100 °C but is not observed at and above 200 °C. At lower temperatures, the $(SCN)_2^{\bullet-}$ yield is relatively large even at KSCN concentrations as low as 1×10^{-4} m; at higher temperatures, however, the $(SCN)_2^{\bullet-}$ is nearly impossible to measure at such a low concentration. Although the solubility of KSCN in supercritical water at 400 °C and 350 atm is unknown, it must be >0.01 m because the absorbance of $(SCN)_2^{\bullet-}$ at 0.05 m KSCN is much higher than at 0.01 m. By assuming the same solubility for KNO_3 and KSCN and using the solubility−water density correlation[22] for KNO_3 at 450−525 °C, the solubility of KSCN at 400 °C and 350 atm would be close to 0.1 m. More evidence is that the solubility of KOH is 1.06×10^{-2} m at 450 °C and 30.4 MPa.[23] The electrolyte solubility has been found to be correlated with density and not with temperature for both KNO_3[22] and KOH.[23] However, it

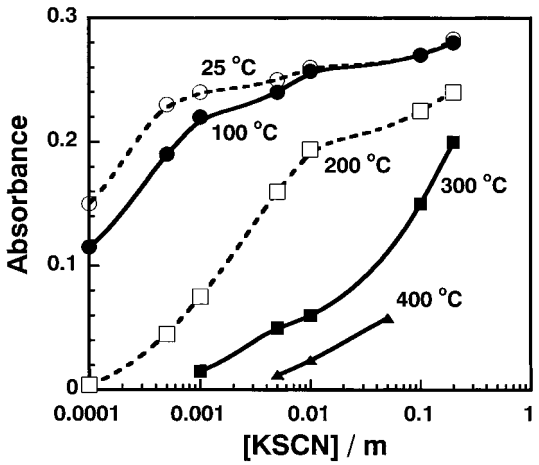

Figure 4. Concentration dependence of the absorption maximum for $(SCN)_2^{\bullet-}$ at various temperatures. Conditions are identical with those in Figure 1.

should be pointed out that the use of concentrated KSCN in supercritical water causes severe corrosion of the reactor wall. Ions of Mo, Ni, and W with unusually high concentrations were detected by inductively coupled plasma (ICP) spectroscopy in the collected effluent from a test using 0.1 m KSCN at 400 °C and 350 atm.

Temperature effects on the KSCN dependence of $(SCN)_2^{\bullet-}$ can be explained by the variation of kinetic parameters involving the $(SCN)_2^{\bullet-}$ formation. In N_2O-saturated SCN^- solutions, the $(SCN)_2^{\bullet-}$ formation processes can be illustrated as follows:

$$H_2O \rightsquigarrow e_{aq}^-, OH^\bullet, H, HO_2^\bullet, ... \quad (1)$$

$$e_{aq}^- + N_2O \rightarrow N_2 + O^{\bullet-} \quad (2)$$

$$O^{\bullet-} + H_2O \rightarrow OH^- + OH^\bullet \quad (3)$$

$$SCN^- + OH^\bullet \rightarrow SCNOH^{\bullet-} \quad (4)$$

$$SCNOH^{\bullet-} \overset{K_1}{\rightleftharpoons} SCN^\bullet + OH^- \quad (5)$$

$$SCN^\bullet + SCN^- \overset{K_2}{\rightleftharpoons} (SCN)_2^{\bullet-} \quad (6)$$

Rate constants for reactions 1−4 are very fast, and reaction 5 lies predominantly to the right in acidic and neutral solutions, so the determining step for the $(SCN)_2^{\bullet-}$ formation is reaction 6. An attempt was made to derive the equilibrium constant, K_2, at high temperatures from the experimental results.

According to Elliot et al.,[13] K_2 as a function of temperature for $(SCN)_2^{\bullet-}$ can be investigated on the basis of the equation

$$A_\infty/A = 1 + \{1/(K_2[SCN^-])\} \quad (7)$$

where A_∞ is the absorbance per unit dose for $(SCN)_2^{\bullet-}$ when all of the $SCN^\bullet$ radicals are converted to $(SCN)_2^{\bullet-}$ and A is the absorbance of unit dose at a certain concentration of SCN^-. For the sake of simplicity, the absorbance at 0.1 m KSCN at each temperature is taken as the A_∞. Because the highest KSCN concentration applied at 400 °C is 0.05 m, the A_∞ is obtained by extrapolating the concentration to 0.1 m.

As the dissociation constant of electrolytes decreases with temperature, the actual SCN^- concentration must be smaller than the added KSCN concentration at high temperatures, especially in supercritical water. The free SCN^- concentration

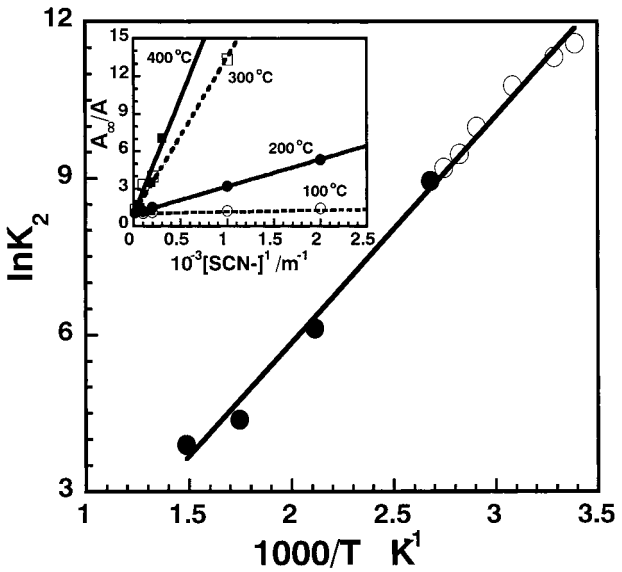

Figure 5. Van't Hoff plot of K_2 over 15−90 °C (○, Elliot et al.[13]) and 100−400 °C (●, this work). Water densities are 0.967 (100 °C), 0.878 (200 °C), 0.743 (300 °C), and 0.475 (400 °C) g/cm^3. Inset: Plots of A_∞/A as a function of [SCN$^-$] for $(SCN)_2^{\bullet-}$ at various temperatures.

was calibrated by assuming the same dissociation constant (K_{Dm}) as for NaCl. The logarithm of the molal dissociation constant for NaCl as a function of temperature and of the logarithm of the water density up to 600 °C is given by Ho et al.[24]

$$\log K_{Dm} = -0.997 + 650.07/T + (10.420 - 2600.5/T)\log \rho_w \quad (8)$$

where T is the Kelvin temperature and ρ_w is the water density. This assumption should make little error in consequence because both NaCl and KSCN are very soluble in water and dissociated into only monovalent ions. The correction is minor for temperatures <300 °C but large at higher temperatures, and it is also very dependent on the KSCN concentration and the water density. For instance, the percentages of KSCN dissociated into free SCN$^-$ are 96 and 76% for solutions with 0.01 and 0.1 m KSCN at 300 °C and 250 atm, respectively, but they are changed to 55 and 31% for solutions with 0.01 and 0.05 m KSCN at 400 °C and 350 atm.

The inset of Figure 5 shows plots of A_∞/A as a function of the reciprocal of [SCN$^-$]. There is a good linearity for all of the lines, being consistent with eq 7. K_2 values at various temperatures are obtained from these curves. K_2 at room temperature was not determined in this work because it has been previously reported,[13] and the determination requires the use of very low KSCN concentration. Figure 5 shows the van't Hoff plot of K_2 using the values obtained in this work in combination with those previous data. Our data over 100−400 °C (with densities of 0.967−0.475 g/cm^3) agree well with those of Elliot et al.[13] over the range 15−90 °C. The enthalpy and entropy obtained from the plot are −36 kJ mol^{-1} and 23 J mol^{-1} K^{-1}, respectively. Because K_2 decreases rapidly with temperature, the $(SCN)_2^{\bullet-}$ yield for a fixed KSCN concentration is decreased. This is why we observed a rapid decrease of $G\epsilon_{max}$ with temperature for 0.01 m KSCN solution.

pH Dependence of $(SCN)_2^{\bullet-}$ and Temperature Dependence of K_1. As already seen in Figure 3, the addition of NaOH to the KSCN solution leads to a decrease in $G\epsilon_{max}$ of $(SCN)_2^{\bullet-}$. This indicates that the backward process of reaction 5 can no longer be neglected at high OH$^-$ concentration. The equilibrium constant of reaction 5, K_1, is expected to vary with temperature. K_1 was reported[25] to be 3.2×10^{-2} M at room temperature. In the present work the temperature dependence of K_1 was studied over the temperature range of 25−400 °C.

When the equilibrium is reached for both reactions 5 and 6, we get

$$[SCN^\bullet] = \frac{K_1[SCNOH^{\bullet-}]}{[OH^-]} = \frac{[(SCN)_2^{\bullet-}]}{K_2[SCN^-]} \quad (9)$$

Of the species indicated in eq 9, only $(SCN)_2^{\bullet-}$ was optically determined. Under conditions at which reactions 5 and 6 lie entirely to the right, concentrations of $SCNOH^{\bullet-}$ and $SCN^\bullet$ are close to zero and $(SCN)_2^{\bullet-}$ is at the highest concentration, C_∞. In this work, the $(SCN)_2^{\bullet-}$ concentration observed in 0.1 m KSCN solution is assumed to be C_∞, being equivalent to $A_\infty/\epsilon l$, where ϵ is the molar absorption coefficient and l is the optical path. Although the $SCN^\bullet$ concentration in 0.1 m KSCN at 300 and 400 °C is not close to zero, it is much smaller than the $(SCN)_2^{\bullet-}$ concentration. Therefore, the assumption will not make a large error in the conclusion. The $(SCN)_2^{\bullet-}$ concentration in 0.01 m KSCN solution is taken as $A/\epsilon l$. According to the material balance

$$[SCNOH^{\bullet-}] + [SCN^\bullet] + [(SCN)_2^{\bullet-}] = C_\infty \quad (10)$$

and $[SCNOH^{\bullet-}]$ can be written as

$$[SCNOH^{\bullet-}] = A_\infty/\epsilon l - A/\epsilon l - [SCN^\bullet] \quad (11)$$

By substituting eq 11 into eq 9 and rearranging the equation, we get

$$[SCN^\bullet] = \frac{K_1(A_\infty/\epsilon l - A/\epsilon l)}{K_1 + [OH^-]} \quad (12)$$

If the temperature, pressure, and SCN$^-$ concentration are fixed but the pH is varied, the ratio of $(SCN)_2^{\bullet-}$ concentrations determined at two different pH values ($[OH^-]_1$ and $[OH^-]_2$) will be

$$\frac{(A_\infty - A_1)/(K_1 + [OH^-]_1)}{(A_\infty - A_2)/(K_1 + [OH^-]_2)} = \frac{A_1}{A_2} \quad (13)$$

In the N_2O-saturated alkaline solutions, the H atom is first converted to e_{aq}^- by the reaction with OH$^-$ and further transformed to $OH^\bullet$ by reacting toward N_2O, so the H atom is an additional $(SCN)_2^{\bullet-}$ source. In ambient liquid water the G value of H is ∼10% of the sum of G values of e_{aq}^- and $OH^\bullet$, so the contribution of the H atom was assumed to be temperature independent and corrected for KSCN solutions with the addition of 0.01 m NaOH. Letting

$$\frac{A_1}{A_2}\frac{A_\infty - A_2}{A_\infty - A_1} = q \quad (14)$$

then we get

$$K_1 = \frac{[OH^-]_2 - q[OH^-]_1}{q-1} \approx \frac{[OH^-]_2}{q-1} \text{ (when } [OH^-]_2 \gg [OH^-]_1) \quad (15)$$

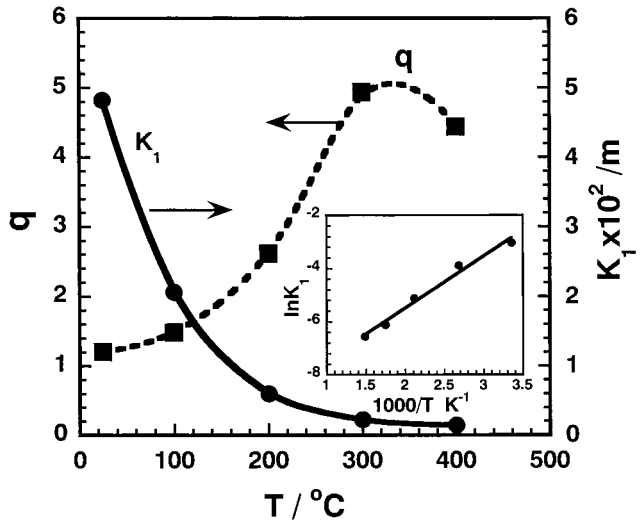

Figure 6. Temperature dependence of q and K_1 over 25−400 °C. Water densities are identical with those indicated in Figure 5. Inset: Van't Hoff plot of K_1.

In eq 15, the OH^- concentration is known and q can be experimentally obtained. The OH^- concentration in 0.01 m KSCN solutions is assumed to be the same as that of pure water and given by $[OH^-]_1$, which can be calculated from the ionic product (k_w) of water. The actual OH^- concentration in 0.01 m KSCN plus 0.01 m NaOH solution is given by $[OH^-]_2$, calculated using the regressed formula for molal dissociation constant of NaOH in H_2O at 25−600 °C[26]

$$\log K_{Dm} = -2.477 + 951.53/T + (9.307 - 3482.8/T) \log \rho_w \quad (16)$$

where T is the Kelvin temperature and ρ_w is the water density. Although the $[OH^-]_1$ increases with temperature and reaches a maximum at ~250 °C, it is smaller than $[OH^-]_2$ by several orders of magnitude and could be neglected in eq 15.

Values of q and K_1 are obtained on the basis of eqs 14 and 15 and using our experimental results. Plots of q and K_1 as a function of temperature over the range of 25−400 °C are shown in Figure 6. It is shown that q increases with temperature up to 300 °C and then decreases slightly at 400 °C. K_1 decreases rapidly with temperature, decreasing from 4.8×10^{-2} to 2×10^{-3} m for a rise from 25 to 400 °C. The inset shows the van't Hoff plot of K_1. The enthalpy and entropy are found to be −16 kJ mol^{-1} and 77 J mol^{-1} K^{-1}, respectively.

Decay and ϵ_{max} of $(SCN)_2^{\bullet-}$. The decay of $(SCN)_2^{\bullet-}$ is usually considered to be a second-order process via reactions 17−19.

$$(SCN)_2^{\bullet-} + (SCN)_2^{\bullet-} \rightarrow (SCN)_3^- + SCN^- \quad (17)$$

$$SCN^{\bullet} + (SCN)_2^{\bullet-} \rightarrow (SCN)_3^- \quad (18)$$

$$SCN^{\bullet} + SCN^{\bullet} \rightarrow (SCN)_2 \quad (19)$$

The overall decay rate constant can be written by

$$2k_t = 2k_{17} + \frac{2k_{18}}{K_2[SCN^-]} + \frac{2k_{19}}{K_2^2[SCN^-]^2} \quad (20)$$

We can see that if $K_2[SCN^-]$ (or $[(SCN)_2^{\bullet-}]/[SCN^{\bullet}]$) is much larger than unit, then the second and third terms on the right of eq 20 can be neglected and $2k_t$ equals $2k_{17}$. Because K_2 is very large at room temperature and reaction 6 lies entirely to the right, the $(SCN)_2^{\bullet-}$ decays predominantly by its bimolecular recombination, reaction 17, given that the SCN^- concentration is not very low. At high temperatures, the $SCN^{\bullet}$ concentration could be comparable to that of $(SCN)_2^{\bullet-}$ due to the decrease of K_2, and reactions 18−19 have to be taken into account. Equation 20 indicates that the $(SCN)_2^{\bullet-}$ should follow a second-order decay at all SCN^- concentrations and at all temperatures. However, we found that the $(SCN)_2^{\bullet-}$ decay obeys second-order kinetics only for temperatures up to 160 °C at relatively high KSCN concentration. The decay could be also fitted by a first-order kinetics even below 150 °C when the KSCN concentration is very low. Equation 20 also indicates that for a fixed temperature, the variation of $[SCN^-]$ may lead to a change in the overall decay rate constant. Indeed, the decay rate of $(SCN)_2^{\bullet-}$ was found to vary with the KSCN concentration at any temperatures considered. If only reactions 17−19 are responsible for the decay of $(SCN)_2^{\bullet-}$, the decay rate of $(SCN)_2^{\bullet-}$ should be slower at lower SCN^- concentrations. However, it was found that in many cases the decay is faster at lower SCN^- concentrations for 300−400 °C, and it is impossible to reproduce the decay profile by the simulation. Therefore, reactions 17−19 are inadequate to describe the decay of $(SCN)_2^{\bullet-}$ at high temperatures, and some additional processes have to be considered.

As is understood, $SCN^{\bullet}$ is the precursor of $(SCN)_2^{\bullet-}$ and its concentration could be large, depending on the temperature and KSCN concentration applied. When the concentration of $SCN^{\bullet}$ is comparable to or even higher than that of $(SCN)_2^{\bullet-}$, the $SCN^{\bullet}$ possibly reacts with other species present in the solution. Consequently, a pseudo-first-order decay of $SCN^{\bullet}$ has to be taken into account, and its role may be important for the $(SCN)_2^{\bullet-}$ decay at high temperatures.

$$SCN^{\bullet} + \text{substance} \rightarrow \text{product} \quad (21)$$

An attempt was made to simulate the $(SCN)_2^{\bullet-}$ decay using the "Facsimile" code. The dose distribution of the electron beam was assumed to be the Gaussian type. A reaction set including 38 reactions for water radiolysis was applied, and the rate constants for these reactions have been compiled by Elliot et al.[27,28] for temperatures up to 300 °C and are extrapolated to 400 °C using the Arrhenius parameters. Reactions involving the formation and decay of $(SCN)_2^{\bullet-}$ and their rate constants are given in Table 1. The experimental conditions and G values of e_{aq}^- and the OH radical at various temperatures used for the simulation are presented in Table 2. Because the Arrhenius parameters of $k_{17}-k_{19}$ are unknown, $k_{17}-k_{19}$ values are assumed to be at the diffusion-controlled limit, estimated by the Stokes−Einstein-based Debye equation, $k_{diff} = 8RT/3\eta$, and using a spin statistical factor of 0.25, where R is the gas constant and η is the viscosity taken from the literature.[32] Reactions 17−19 were found[13] to be essentially diffusion controlled over the temperature range of 15−90 °C, and in this work the overall second-order decay rate constants ($2k_t$) for 0.01 m KSCN solution were also found to be the same as k_{diff} up to 160 °C. At temperatures >200 °C, the $(SCN)_2^{\bullet-}$ does not obey a second-order kinetics so the fitted $2k_t$ is higher than k_{diff}. The assumption of $k_{17}-k_{19}$ to be at the diffusion-controlled limit up to 400 °C is reasonable because more recently a study[7] showed that diffusion-controlled reactions in normal liquids also occur at the normal diffusion-controlled limit in supercritical water. For other reactions, if their values are unknown, the diffusion-controlled limit rate is applied. The rate constant for the $SCN^{\bullet}$ decay was adjusted to make sure that the simulated line agrees well with the measured

TABLE 1: Rate Constants (M^{-1} s^{-1} or s^{-1}) and Equilibrium Constants Used for the Simulation of the $(SCN)_2^{\bullet-}$ Decay at 25−400 °C[a]

(a) $e_{aq}^- + N_2O \rightarrow O^- + N_2$	9.6×10^9 (25 °C), log $A = 13.3$, $E = 19$ kJ/mol (25−200 °C);[29] $T > 200$ °C, diffusion-control limit
(b) $O^- + H_2O \rightarrow OH + OH^-$	data taken from Elliot et al.[27]
(c) $OH + SCN^- \rightarrow SCNOH^{\bullet}$	1.0×10^{10} (25 °C), log $A = 11.95$, $E = 11$ kJ/mol, 25−200 °C;[30] $T > 200$ °C, diffusion-control limit
(d) $SCNOH^{\bullet-} \rightleftarrows SCN^{\bullet} + OH^-$	$K_1 = 4.8 \times 10^{-2}$ m (25 °C), $\Delta H = -16$ kJ mol^{-1}, $\Delta S = -77$ J mol^{-1} K^{-1} at 25−400 °C
(e) $SCN^{\bullet} + SCN^- \rightleftarrows (SCN)_2^{\bullet-}$	$K_2 = 1 \times 10^5$ m^{-1} (25 °C), $\Delta H = -36$ kJ mol^{-1}, $\Delta S = -23$ J mol^{-1} K^{-1} at 25−400 °C
(f) $(SCN)_2^{\bullet-} + (SCN)_2^{\bullet-} \rightarrow (SCN)_3^- + SCN^-$	25 °C, $2k = 2.2 \times 10^9$, diffusion controlled at 25−400 °C
(g) $SCN^{\bullet} + (SCN)_2^{\bullet-} \rightarrow (SCN)_3^-$	the same as for (f)
(h) $SCN^{\bullet} + SCN^{\bullet} \rightarrow (SCN)_2$	the same as for (f)
(i) $SCN^{\bullet}$ + substance → products	25 °C, 3.0×10^5 s^{-1}; 100 °C, 6.0×10^5 s^{-1}; 200 °C, 9.0×10^5 s^{-1}; 300 °C, 1.4×10^6 s^{-1}; 400 °C, 5.0×10^6 s^{-1}

[a] Another 38 reactions including reaction b for water radiolysis are also used in the simulation, see refs 27 and 28.

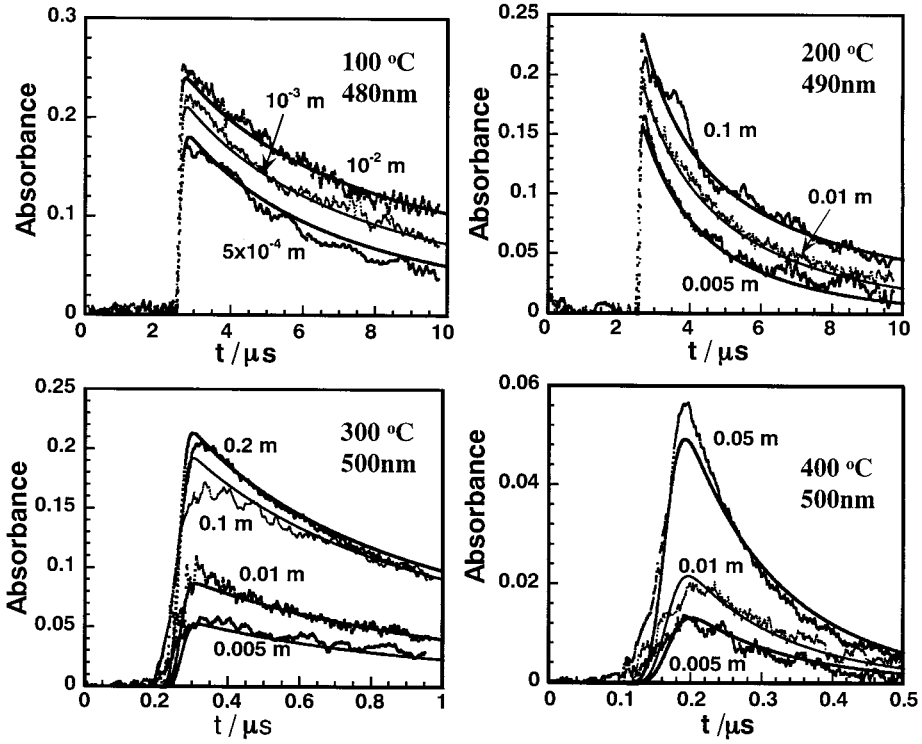

Figure 7. Comparison of experimentally determined and simulated (bold solid lines) time profiles of $(SCN)_2^{\bullet-}$ at various temperatures. KSCN concentrations are indicated, and other conditions are the same as shown in Figure 1.

TABLE 2: Experimental Conditions and $G(e_{aq}^-)$ and $G(OH^{\bullet})$ over 25−400 °C

T (°C)	pressure (atm)	water density (g/cm^3)	$G(e_{aq}^-)$[a] (μmol J^{-1})	$G(OH)$[a] (μmol J^{-1})	pK_w[b] $(mol/kg)^2$
25	200	1.008	0.280	0.296	13.92
100	200	0.968	0.300	0.348	12.12
200	200	0.876	0.336	0.422	11.04
300	250	0.743	0.370	0.496	10.97
400	350	0.475	0.406	0.571	13.06

[a] The data at 0−300 °C are taken from Elliot[27] and further extrapolated to 400 °C. [b] Calculated based on the equation of Quist:[31] $\log K_w = -3.74 - 3050/T + 14.8 \log \rho$, where T is Kelvin temperature and ρ is the water density.

decay profile of $(SCN)_2^{\bullet-}$ for solutions with various SCN^- concentrations at each temperature. In the simulation, the molal SCN^- concentration and the molal equilibrium constants are changed to molar units by taking into account the water density.

For solutions with high SCN^- (>0.01 m), the rate constant has been calibrated for the ionic strength effects based on the equation[33]

$$\ln k = \ln k_0 + 8.36 \times 10^6 Z_a Z_b I^{0.5}/[(1 + I^{0.5})(\epsilon T)^{1.5}] \quad (22)$$

where I is the ionic strength and ϵ is the relative dielectric constant at temperature T (K). This formula has also been used by Buxton et al.[34,35] for the calibration of rate constants in high-temperature water. This calibration is important for temperatures >300 °C, at which ϵ is considerably decreased.

Figure 7 shows the simulated curves together with the experimental ones for the $(SCN)_2^{\bullet-}$ decay at 100−400 °C. It is clear that the time profiles of $(SCN)_2^{\bullet-}$ are reproduced well by the simulation for any temperatures considered. Because the simulated results are the time-dependent molar concentrations of $(SCN)_2^{\bullet-}$ whereas the experimental curves are the time-dependent absorption of $(SCN)_2^{\bullet-}$, the simulation data are enlarged by a suitable factor at each temperature for normalization. To check the validity of the rate constants and equilibrium constants indicated in Table 1, at least three runs with different KSCN concentrations at each temperature are tested, and all of the results are satisfied. The simulated curves for room temperature are not shown in Figure 7 because the rate constants have been well established.

ϵ_{max} of $(SCN)_2^{\bullet-}$. According to the Lambert−Beer law, the absorbance maximum of $(SCN)_2^{\bullet-}$ is given by $A_{max} = \epsilon_{max} cl$, where c is the molar concentration and ϵ_{max} is the molar absorption coefficient. The enlarging factors applied for nor-

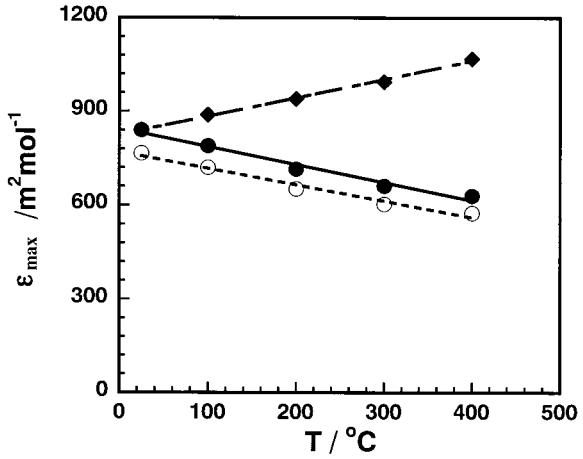

Figure 8. Molar absorption coefficient of $(SCN)_2^{\bullet-}$ as a function of temperature: (●) using the $G(e_{aq}^-)$ and $G(OH^\bullet)$ values shown in Table 2; (○) calibrated using $G(OH^\bullet) = 0.63$ μmol/J at room temperature in N_2O-saturated KSCN solution as compared to $G(e_{aq}^-) + G(OH^\bullet) = 0.57$ μmol/J but assuming the same temperature dependence as shown in Table 2; (◆) assuming the temperature independence of G values.

malization of the simulated curves in Figure 7 are actually equal to $\epsilon_{max}l$ for profiles depicted at the absorption peak. As the optical path is 1.5 cm in this work, ϵ_{max} can be obtained. The so-obtained ϵ_{max} as a function of temperature is shown in Figure 8. The ϵ_{max} decreases with temperature, and its value at 400 °C is ~70% of that at room temperature. Because the increase of G values of $OH^\bullet$ and e_{aq}^- is faster than the decease of ϵ_{max}, $G\epsilon_{max}$ should increase continuously with temperature if all of the $OH^\bullet$ radicals are converted to $(SCN)_2^{\bullet-}$. However, a decrease of $G\epsilon_{max}$ with temperature was experimentally observed above 150 °C (Figure 3) because the $SCN^\bullet$ exists in a large amount in high-temperature water as does the $(SCN)_2^{\bullet-}$. Owing to the limited KSCN solubility and the decrease of K_2 at high temperatures, it is impossible to convert all of the $SCN^\bullet$ to $(SCN)_2^{\bullet-}$, although the $OH^\bullet$ radicals can be completely scavenged by SCN^- and transformed to $SCN^\bullet$.

Conclusion

The temperature dependence of the absorption spectrum, yield, and decay for $(SCN)_2^{\bullet-}$ has been examined by the pulse radiolysis technique. The experiment reveals a red shift of the spectrum of $(SCN)_2^{\bullet-}$ with temperature. The equilibrium constant K_2 for the reaction $SCN^\bullet + SCN^- \rightleftarrows (SCN)_2^{\bullet-}$ decreases considerably with increasing temperature, from 1×10^5 m^{-1} at room temperature to 30 m^{-1} at 400 °C, so the $G\epsilon_{max}$ observed at high temperatures is very dependent on the SCN^- concentration. At high temperatures at which K_2 is small or at room temperature with very low SCN^- concentration, the $SCN^\bullet$ concentration could be high and the decay of $SCN^\bullet$ must be considered. Under these conditions the decay of $(SCN)_2^{\bullet-}$ does not obey second-order kinetics and a pseudo-first-order decay of $SCN^\bullet$ has to be considered to account for the decay of $(SCN)_2^{\bullet-}$. The simulation using the known and some assumed rate constants reproduces well the decay profile of $(SCN)_2^{\bullet-}$ over the temperature range investigated. Although the 10 mM KSCN solution is usually used as the dosimeter in pulse radiolysis at room temperature, it is not suitable for high-temperature water. We expect the results of the present work are also helpful for understanding of the behavior of other dimer radical anions in high-temperature water, especially for the temperature effect on equilibrium constants of the dimer anion formation.

Acknowledgment. This work was supported by Japan Society for the Promotion of Science under Contract JSPS-RFTF 98P00901.

References and Notes

(1) Chlistunoff, J. B.; Johnston, K. P. *J. Phys. Chem. B* **1998**, *102*, 3993.
(2) Bennett, G. E.; Johnston, K. P. *J. Phys. Chem.* **1994**, *98*, 441.
(3) Masten, D. A.; Foy, B. R.; Harradine, D. M.; Dyer, R. B. *J. Phys. Chem.* **1993**, *97*, 8557.
(4) Hoffmann, M. M.; Conradi, M. S. *J. Am. Chem. Soc*. **1997**, *119*, 3811.
(5) Hoffmann, M. M.; Darab, J. G.; Palmer, B. J.; Fulton, J. L. *J. Phys. Chem. A* **1999**, *103*, 8471.
(6) Green, S.; Xiang, T.; Johnston, K. P.; Fox, M. A. *J. Phys. Chem*. **1995**, *99*, 13787.
(7) Kremer, M. J.; Connery, K. A.; DiPippo, M. M.; Feng, J.; Chateauneuf, J. E.; Brennecke, J. F. *J. Phys. Chem. A* **1999**, *103*, 6591.
(8) Ferry, J. L.; Fox, M. A. *J. Phys. Chem. A* **1999**, *103*, 3438.
(9) Ferry, J. L.; Fox, M. A. *J. Phys. Chem. A* **1998**, *102*, 3705.
(10) Wu, G.; Katsumura, Y.; Muroya, Y.; Terada, Y.; Li, X. *Chem. Phys. Lett*. **2000**, *325*, 531.
(11) Takahashi, K.; Cline, J. A.; Bartels, D. M.; Jonah, C. D. *Rev. Sci. Instrum*. **2000**, *71*, 3345.
(12) Nielsen, S. O.; Michael, B. D.; Hart, E. J. *J. Phys. Chem*. **1976**, *80*, 2482.
(13) Elliot, A. J.; Sopchyshyn, F. C. *Int. J. Chem. Kinet*. **1984**, *16*, 1247.
(14) Buxton, G. V.; Stuart, C. R. *J. Chem. Soc., Faraday Trans*. **1995**, *91*, 279.
(15) Hill, P. G. *J. Phys. Chem. Ref. Data* **1990**, *19*, 1233.
(16) Michael, B. D.; Hart, E. J.; Schmidt, K. H. *J. Phys. Chem.* **1971**, *75*, 2798.
(17) Christensen, H.; Sehested, K. *J. Phys. Chem.* **1986**, *90*, 186.
(18) Shiraishi, H.; Katsumura, Y.; Hiroishi, D.; Ishigure, K.; Washio, M. *J. Phys. Chem.* **1988**, *92*, 3011.
(19) Schuler, R. H.; Patterson, L. K.; Janata, E. *J. Phys. Chem*. **1980**, *84*, 2088.
(20) Sauer, Jr., M. C.; Jonah, C. D.; Schmidt, K. H.; Naleway, C. A. *Radiat. Res*. **1983**, *93*, 40.
(21) Chitose, N.; Katsumura, Y.; Domae, M.; Zuo, Z.; Murakami, T. *Radiat. Phys. Chem.* **1999**, *54*, 385.
(22) Dell'Orco, P.; Eaton, H.; Reynolds, T.; Buelow, S. *J. Supercrit. Fluids* **1995**, *8*, 217.
(23) Wofford, W. T.; Dell'Orco, P. C.; Gloyna, E. F. *J. Chem. Eng. Data* **1995**, *40*, 968.
(24) Ho, P. C.; Palmer, D. A.; Mesmer, R. E. *J. Solution Chem*. **1994**, *23*, 997.
(25) Behar, D.; Bevan, P. L. T.; Scholes, G. *J. Phys. Chem*. **1972**, *76*, 1537.
(26) Ho, P. C.; Palmer, D. A. *J. Solution Chem*. **1996**, *25*, 711.
(27) Elliot, A. J. Rate Constants and g-Values for the Simulation of the radiolysis of Light Water Over the range 0−300 °C; AECL Report AECL-11073, COG-94-167; 1994.
(28) Elliot, A. J.; Quellette, D. C.; Stuart, C. R. The Temperature Dependence of the Rate Constants and yields for the Simulation of the Radiolysis of Heavy Water; AECL Report AECL-11658, COG-96-390I; 1996.
(29) Elliot, A. J. *Radiat. Phys. Chem*. **1989**, *34*, 753.
(30) Elliot, A. J.; Simsons, A. S. *Radiat. Phys. Chem.* **1984**, *24* (2), 229.
(31) Quist, A. S. *J. Phys. Chem.* **1970**, *74*, 3396.
(32) Sengers, J. V.; Waston, J. T. R. J. *Phys. Chem. Ref. Data* **1986**, *15*, 1291.
(33) Weston, R. E.; Schwarz, H. A. *Chemical Kinetics*; Prentice-Hall: Englewoodd Cliffs, NJ, 1972.
(34) Buxton, G. V.; Mackenzie, S. T. *J. Chem. Soc., Faraday Trans*. **1992**, *88*, 2833.
(35) Elliot, A. J.; McCracken, D. R.; Buxton, G. V.; Wood, N. D. *J. Chem. Soc., Faraday Trans.* **1990**, *86*, 1539.